The effect of Cu content on corrosion, wear and tribocorrosion resistance of Ti-Mo-Cu alloy for load-bearing bone implants

Xin Lu [a], Dawei Zhang [a], Wei Xu [a, b, c *], Aihua Yu [a], Jiazhen Zhang [a], Maryam Tamaddon [b], Jianliang Zhang [d], Xuanhui Qu [a], Chaozong Liu [b], Bo Su [c]

[a] Beijing Advanced Innovation Center for Materials Genome Engineering, Institute for Advanced Materials and Technology, State Key Laboratory for Advanced Metals and Materials, University of Science and Technology Beijing, Beijing 100083, China.

[b] Institute of Orthopaedic & Musculoskeletal Science, University College London, Royal National Orthopaedic Hospital, Stanmore HA7 4LP, UK

[c] Bristol Dental School, University of Bristol, Bristol BS1 2LY, UK

[d] School of Metallurgical and Ecological Engineering, University of Science and Technology Beijing, Beijing 100083, China

Abstract

In this study, the effects of Cu content on wear, corrosion, and tribocorrosion resistance of Ti-10Mo-xCu alloy were investigated. Results revealed that hardness of Ti-10Mo-xCu alloy increased from 355.1±15.2 HV to 390.8±17.6 HV by increasing Cu content from 0% to 5%, much higher than CP Ti (106.6±15.1 HV) and comparable to Ti64 (389.7±13.9 HV). With a higher Cu content, wear and tribocorrosion resistance of Ti-10Mo-xCu alloys were enhanced, and corrosion resistance showed an initial increase with a subsequent decrease. Wear mechanisms under pure mechanical wear and tribocorrosion conditions of Ti-10Mo-xCu alloys were a combination of delamination, abrasion and adhesion wear.

Keywords

* **Corresponding author:** Wei Xu, Tel.: +86 10 6233 3981; E-mail address: xuweicool@126.com.

Ti-10Mo-xCu alloys, wear, corrosion, tribocorrosion, bone implants

1. Introduction

Over one million knee and hip replacements surgeries take place every year worldwide due to an aging population and injuries to the bone tissue and joint from trauma and sports accidents [1, 2]. Thus, there exists an increasing demand for load-bearing bone implants. Ti-based alloys, owing to their high strength, low elastic modulus, excellent corrosion resistance, and biocompatibility have received growing interests [3-6]. However, currently widely used Ti-based materials, such as commercially pure titanium (CP Ti) and Ti-6Al-4V (Ti64) alloys, still have some limitations. Firstly, the elastic modulus of CP Ti (~110 GPa) and Ti64 (~120 GPa) are substantially higher than human bones (e.g. 0.01-3 GPa for trabecular bone and 3-30 GPa for cortical bone) [7]. This elastic modulus mismatch could cause a stress shielding effect, which leads to bone resorption around the implants and ultimately the failure of implantation. Secondly, CP Ti has relatively low strength and wear resistance, which may greatly shorten the implant's service life. Thirdly, Ti64 alloy may have some negative health concerns in regards to its long-term implantation, such as mental disorder, hypomnesia, and Alzheimer's disease, because of the release of aluminum (Al) or vanadium (V) ions [8]. Lastly, bacterial infections could still occur even if surgeries are carried out under strict aseptic conditions, which could lead to revisions, resulting in extra pain and cost to patients and healthcare providers [9, 10]. Therefore, new-generation Ti alloys with higher strength, excellent biocompatibility, lower elastic modulus, and the antibacterial property are of urgent need. We recently developed a new Ti-Mo-Cu alloy that 1-5 wt% Cu was added in Ti-10Mo alloys due to the excessive Cu will deteriorate the ductility and also may result in cytotoxicity [11], and the effects of Cu content on the tensile properties, cytocompatibility, and bacterial inhibitory ability of Ti-10Mo alloys were investigated. The results indicated that this kind of alloys has promising mechanical properties, cytocompatibility, and antibacterial property.

For load-bearing bone implants, corrosion, wear, and the interaction of mechanical loading and chemical/electrochemical reactions, or so-called tribocorrosion are also important properties. It is well known that Ti-based alloys are surrounded by body fluids containing a variety of complex electrolytes (e.g. proteins and chloride ion) when it is implanted into the human body [12, 13], which leads to corrosion. In addition, there are also relative motions, such as sliding and fretting, between the implant and bone. Sometimes, these two phenomena can occur simultaneously [14, 15]. Under tribocorrosion conditions, the deterioration of the materials is exacerbated, and the material loss is often higher than the sum of the material loss by corrosion or wear alone, because of the synergistic effect between pure mechanical wear and electrochemical corrosion [16, 17]. Additionally, metal ion release can also be accelerated, and more debris can be generated under the tribocorrosion conditions, which may induce cytotoxicity [18-21]. Therefore, it is crucial to investigate the corrosion, wear, and tribocorrosion properties of Ti-Mo-Cu alloy, which have been rarely reported in the literature.

The objectives of this study were to investigate the effect of Cu content on the wear, corrosion, and tribocorrosion properties of Ti-10Mo-xCu alloy, and to clarify the mechanisms of interactions between pure mechanical wear and corrosion of Ti-10Mo-xCu alloy, so as to provide basic guidance for its practical application as load-bearing bone implants.

2. Materials and methods

2.1 Materials and specimen's preparation

Ti-10Mo-xCu (x=0,1,3,5) alloys were fabricated by powder metallurgy (PM) using commercial Ti, Mo, and Cu powders (purity ≥ 99.9%). The fabrication process was as follows: (1) the Ti powders were coated by polyethylene glycol (PEG) to decrease the oxygen content to enhance the mechanical properties. The coated process of Ti powders by PEG is as follows: 1 g PEG was added into 50 mL dichloromethane (CH_2Cl_2) and magnetically stirred for 1 h until complete dissolution. Then 100 g HDH Ti powder was added into the PEG-dichloromethane solution at room temperature and stirred it for 0.5 h. The entire process was carried out in an Ar protective glove box. Afterward, the mixed solution was taken out and heated at 50 °C in a fume hood for complete evaporation of the dichloromethane. After being dried in a vacuum oven, the PEG-coated Ti powder was obtained; (2) the coated Ti powders were mixed with Cu and Mo powders in a nominal composition of Ti-10Mo-xCu (x=0,1,3,5) in a blender for 6h with the rotation speed of 100 rpm/min. (3) the mixed powders were compressed into a cylindrical compact by cold isostatic compaction at 200 MPa; (4) the cylindrical compacts were sintered at different temperatures ranging from 1360 ℃ to 1400 ℃ under argon (Ar) atmosphere in a tube furnace. The detailed information on the particle size of the powders and sintering processes were described elsewhere [22, 23].

2.2 Tribocorrosion and pure mechanical wear testing

The tribocorrosion test of Ti-10Mo-xCu alloy was performed by a ball-on-plate tribometer (UMT-Ⅱ) by reciprocating slide integrated with an electrochemical workstation in phosphate-buffered saline (PBS) solution at 37 ± 0.5 ℃. The electrochemical workstation consisted of a working electrode (specimens), a reference electrode (saturated calomel electrode, SCE), and a counter electrode (platinum grid). The components of the PBS solution were NaCl 8 g/L, KCl 0.2 g/L, KH_2PO_4 0.2 g/L, Na_2HPO_4 1.15 g/L, and the pH was 7.2. The volume of electrolytes was 100 mL. Specimens were cut into rectangular plates (20 × 6 × 2 mm^3) by electrical discharge machining (EDM) and embedded in epoxy resin. The exposed areas were 120 mm^2. The specimens were ground with SiC abrasive paper to 2000 grit and then polished to the mirror surface. Finally, the samples were ultrasonic cleaned with absolute ethyl alcohol and dried in a vacuum desiccator at room temperature. As-cast CP Ti and Ti64 alloy were tested simultaneously as references. The slip frequency was 1 Hz, and the stroke lengths were 15 mm. The applied load was 1.5 N, which led to a Hertzian contact pressure of 343-349 MPa for all alloys. The counter material was ZrO_2 ball, and the diameter was 10 mm. Also, to eliminate electrochemical corrosion, the tribocorrosion measurement was also performed under an applied potential of -0.8 V (vs. SCE), namely pure mechanical wear. The coefficient of friction (COF) and open circuit potential (OCP) values before, during, and after sliding were continuously recorded. Before sliding, the potential of each specimen was stabled by immersing the specimens into the solution for 2h. After the potential was stabled, the sliding began for 1h. Afterward, the OCP values were recorded for another 0.5h continuously. For tribocorrosion and pure mechanical wear tests, 5 experiments were repeated to verify the reproducibility.

2.3 Electrochemical corrosion testing

Different electrochemical measurements were performed in a conventional three-electrode system according to the ASTM G59-97 standard [24] in PBS solution at 37 ± 0.5 °C. The size and preparation process of tested specimens were the same as the tribocorrosion tests. Prior to the potentiodynamic polarization (PD) measurements, samples were stabilised in the PBS solution for 2h. After that PD curves with (dynamic corrosion) and without (static corrosion) sliding was measured. The scan rate was 0.5 mV/s while the scan scale was -0.3-2 V vs OCP. The corrosion potential (E_{corr}) and the passive current density (i_p, determined at 0.5 V) were obtained from PD curves. For the electrochemical test, 5 experiments were repeated to verify the reproducibility.

2.4 Characterisation

A Dmax-RB X-ray diffractometer (Rigaku, Tokyo, Japan) with Cu target (λ = 0.15406 nm) was used to analyse the phase constituents of the alloys. The Vickers micro-hardness was tested using a Buehler Micromet 2100 tester with a 0.5 N load based on the ASTM E384-11 standard [25]. Ten points were tested for each sample and the average value was obtained.

After tribocorrosion and pure mechanical wear tests, the samples were ultrasonically cleaned in ethyl alcohol absolute for 10 mins and dried in a vacuum desiccator at room temperature. Scanning electron microscope (SEM, JSM-6480LV, Japan) equipped with n energy dispersive X-ray spectrometry (EDS) was used to analyse the surface topography and chemical composition of the alloys. The three-dimensional (3D) topographies of all specimens were observed using the white light interference microscope (Contour GTK, Bruker), and the wear volume was obtained.

2.5 Calculation

Repassivation rate for a certain period was calculated by the formula (1) [26], as follows:

$$\Delta E = K_1 \times \log t + K_2 \qquad (1)$$

where t is a certain time after interrupting sliding, which is usually 300 s; ΔE is the potential variation during the time of t, V; K_1 is a value that represented the repassivation rate; K_2 is the constant, which is determined by the solution, and 0.1 for PBS.

The total material loss rate (W, mm/y) and the pure mechanical wear rate (W_0, mm/y), namely the tribocorrosion and pure mechanical wear testing, were calculated by the following equation (2) according to ASTM G119-09 [27]:

$$Wear \cdot rate = \frac{\Delta \mathrm{m}}{S \times \rho \times \mathrm{t}} \times 24\left(\frac{h}{d}\right) \times 365\left(\frac{d}{y}\right) \qquad (2)$$

where, Δm is the wear loss, obtained indirectly from the laser scanning confocal microscopy, g; S is the area of worn surface, mm^2; ρ is specimen density, g/cm^3; t is test time, h.

3. Results and discussion

3.1 Phase constituents and Vickers micro-hardness

XRD is used to analyse the phase constituents of Ti-10Mo-xCu using CP Ti, and Ti64 alloy as control samples. In Fig. 1(a), Ti-10Mo and Ti-10Mo-1Cu alloys were characterized by α and β phases, while Ti-10Mo-3Cu and Ti-10Mo-5Cu showed a small amount of Ti_2Cu co-existing with α and β phases. In addition, the content of Ti_2Cu increased with an increase in Cu content, which was in agreement with the previous result [28]. Furthermore, as the Cu content increased, the intensity of the β phase became gradually higher, indicating that more β phases had been generated. This result can be explained by the well-known stabilizing effect of Cu towards the β phase. For the CP Ti and Ti64 alloy, they consisted of α phase and α+β phases, respectively.

Fig.1(b) presents the Vickers micro-hardness values of Ti-10Mo-xCu with different Cu content, alongside with CP Ti, and Ti64 alloy. It can be seen that the micro-hardness of Ti-10Mo-xCu alloys increased from 355.1±15.2 HV to 390.8±17.6 HV when the Cu content increased from 0 to 5 wt.%, which are much higher than that of the CP Ti (106.6±15.1 HV) and comparable to the Ti64 alloy (389.7±13.9 HV). This is mainly caused by solid strengthening by Mo and Cu elements [29, 30]. In addition, the Ti_2Cu phase, which is a hard brittle intermetallic, also can improve the strength of the Ti-Mo-Cu alloys [31]. As a result, the Ti-10Mo-5Cu alloy exhibits the highest hardness of 390.8 HV.

3.2 Wear behaviour

3.2.1 COF

The COF values of Ti-10Mo-xCu alloys, alongside with CP Ti, and Ti64 alloy under pure mechanical wear and tribocorrosion conditions are shown in Fig. 2. It can be observed that the COF values exhibited a relatively steady-state with local fluctuations under pure mechanical wear and tribocorrosion conditions. The COF of Ti-10Mo-xCu alloys decreased with the Cu content, due to the formation of Ti-Cu intermetallic compounds, e.g. Ti_2Cu in the present study [32]. Comparing with Fig. 2(a) and (b), it can be seen that the COF of all alloys under the tribocorrosion condition were higher than those under pure mechanical wear condition. Under the tribocorrosion condition, there is an interaction between wear and corrosion, which will result in stronger friction. This friction can lead to higher COF values. This is agreed with Zhang's study, who demonstrated that during tribocorrosion the COF of the nickel-aluminium bronze (NAB) was higher compared with that observed without corrosion [33]. The Ti-10Mo-5Cu alloy presented the lowest average COF under pure mechanical wear (0.48±0.02) and tribocorrosion conditions (0.58±0.03), much lower than those of the Ti64 alloy (0.51±0.04 and 0.62±0.03, respectively) and CP Ti (0.75±0.07 and 0.95±0.09, respectively).

3.2.2 The morphologies of wear tracks

The white light interference microscope was used to analyse the 3D morphologies of the wear tracks after pure mechanical wear and tribocorrosion tests (Fig. 3). It can be seen that the surface of all samples exhibited similar morphologies, namely, all samples had obvious furrows and severe plastic deformation. In addition, it can be found that the wear tracks of Ti-10Mo-xCu alloys became shallower and narrower with an increasing Cu content due to the increase of hardness. The Ti-10Mo-5Cu alloy exhibits the smallest width of 0.454±0.05 mm and 0.821±0.04 mm under pure mechanical wear and tribocorrosion conditions, respectively, smaller than those of the CP Ti significantly

(0.514±0.03 mm and 1.17±0.09 mm) and comparable to those of the Ti64 alloy (0.458±0.06 mm and 0.829±0.05 mm).

3.2.3 Wear rate

Fig. 4 shows the wear rates under pure mechanical wear and tribocorrosion conditions calculated by equations (1) and (3). The wear rate of Ti-10Mo-xCu alloys decreased gradually with the increasing Cu content, and the Ti-10Mo-5Cu alloy exhibited the lowest wear rate of 8.25033±0.11 mm/y and 4.234±0.06 mm/y under tribocorrosion and pure mechanical wear tests, respectively, lower than those of the CP Ti (20.56984±0.09 mm/y and 11.49±0.08 mm/y) and comparable to those of the Ti64 alloy (8.54568±0.04 mm/y and 4.5625±0.03 mm/y). Furthermore, it can be found that the alloys exhibit higher wear rates under the tribocorrosion than those values under pure mechanical wear conditions. This was mainly because the passive film formed on the surface was loose and coarse under tribocorrosion, which can be easily peeled off [34].

3.2.4 Wear track surface analysis and wear mechanisms

In order to further characterise the wear mechanisms, the surfaces of the wear tracks on all alloys after pure mechanical wear and tribocorrosion tests were examined using SEM. In Fig. 5, parallel grooves to the sliding direction indicated that the occurrence of abrasive wear [35]. Meanwhile, there were some laminar tearing on the wear track due to the delamination of the alloys caused by rubbing against the ZrO_2 ball, suggesting that the delamination wear also existed [36]. In this study, the ZrO_2 ball was used as counter material, which has a higher hardness (~700 HV) than all the specimens (100-400 HV). During the sliding motion, the harder ZrO_2 ball can be embedded into the softer alloys under the applied load, resulting in abrasive wear and provoking an increase in wear rate [21, 37]. Additionally, two kinds of zones, namely dark and grey zone, can be observed from the back-scattered electron and secondary electron (BSE-SE) images. To identify these two zones, an EDS analysis was carried out. Taking Ti-10Mo-5Cu alloy as an example (Fig. 5(d)), the EDS results indicated that the grey zone (Z1) consisted of Ti, Mo, and Cu elements only, while the dark zone (Z2) possessed much higher O content, suggesting the existence of oxides of TiO_2, MoO_3, and CuO_2. As a result of squeezing and scraping between the alloys surface and the counter material, some oxidised wear debris were generated under sliding. The oxidised debris accumulated gradually with the continued sliding, and finally adhered to the surface, indicating that the occurrence of adhesion wear. Similar results were observed for the CP Ti and Ti64 alloy, i.e. oxides such as TiO_2 and TiO_2-Al_2O_3 are presented in the dark area (Fig. 5(e) Z3 and (f) Z4). The results under tribocorrosion conditions (Fig. 5(g)-(l)) were similar to those under pure mechanical wear. Therefore, it is reasonable to assume that the wear mechanisms for all the alloys under both conditions were a combination of delamination, abrasion, and adhesion wear.

3.3 Electrochemical analyses

3.3.1 Open circuit potential

Fig. 6 shows the OCP of Ti-10Mo-xCu, CP Ti, and Ti64 alloy before the static corrosion test in PBS solution at 37 ± 0.5 °C. It can be observed that all the alloys showed a similar tendency where the E_{ocp} moved towards more positive values with the extended immersion time until they became quasi-stationary. The E_{ocp} values of all the Ti-10Mo-xCu were more positive than that of CP Ti and Ti64 alloy, meaning that the addition of Cu has decreased the tendency of corrosion. Among them, the Ti-10Mo-3Cu exhibits the most positive potential (-0.084±0.02 V vs. SCE), indicating that a more passive surface may have formed on this alloy.

Fig. 7 presents the OCP values for Ti-10Mo-xCu, alongside with the CP Ti and Ti64 alloy before, during, and after sliding in PBS solution at 37 ± 0.5 °C. Similar to the OCP values before the static corrosion test, the values before sliding increased gradually, and finally reached a quasi-stationary state after some time. With the start of sliding, the OCP shifted abruptly towards more negative values. After that, it increased within several seconds and then fluctuated within small amplitudes around a value before the sliding stopped. In general, the OCP is a mixed potential of active areas and passive unworn areas and is affected by the ratio of these two areas [38, 39]. It should be noted that the surface of all the samples formed stable oxide films before sliding. When sliding started the formed mixed oxide films were damaged by the mechanical attack at the contact region [40, 41], leading to a sharp decrease in the OCP. However, when the de-passivation and passivation rates reached a dynamic equilibrium, the OCP values became relatively stable. The OCP value of Ti-10Mo-xCu alloys increased initially and then decreases during sliding with increasing Cu, which suggested that the corrosion tendency decreased at first and then increased. The Ti-10Mo-3Cu alloy demonstrated the noblest OCP (-0.41±0.03 V vs. SCE), higher than that of CP Ti (-0.66±0.05 V vs. SCE) and Ti64 alloy (-0.51±0.04 V vs. SCE). This result indicated that the Ti-10Mo-3Cu also were least likely to be corroded under the tribocorrosion condition. After the sliding stopped, the OCP values remarkably increased and gradually recovered to the original values, indicating the re-passivation of the worn surface [42].

Similar to the results during sliding, the OCP values of Ti-10Mo-xCu alloys after sliding increased firstly and subsequently decreased with increasing Cu. The Ti-10Mo-3Cu alloy exhibited the highest potential of -0.03±0.01 V vs. SCE compared with the CP Ti (-0.221±0.04 V vs. SCE) and Ti64 alloy (-0.158±0.03 V vs. SCE). The K_1 value that represented repassivation ability was calculated based on the formula (1), as shown in Fig. 8. It was observed that with the increase of Cu content, the value of K_1 of Ti-10Mo-xCu alloys increased gradually, and it showed the maximum value of 0.121±0.003 when adding 5% Cu content. While continuing to rise Cu content, the value of K_1 decreased slightly to 0.112±0.002. In comparison with the K_1 value of pure Ti (0.068±0.003) and Ti-6Al-4V (0.109±0.002), K_1 of Ti-10Mo-3Cu alloy was greater indicating that the alloy had the highest re-passivation capability after sliding.

3.3.2 Potentiodynamic polarisation

Fig. 9 shows the PD curves of Ti-10Mo-xCu, alongside with CP Ti and Ti64 alloy under static corrosion and tribocorrosion conditions. No significant difference was found for the cathodic branches for all the alloys, indicating that a similar cathodic reaction occurred on the surface of Ti-10Mo-xCu, CP Ti, and Ti64 alloy. The anodic branches under both static corrosion and tribocorrosion conditions exhibited similar curves, characterised by three regions. Taking the Ti-10Mo-3Cu alloy under static corrosion as an example (Fig. 9a), in the first region, the current density increases with the scanning potential until it reached the second region. In the second region, the current density remained almost constant with the increase in the scanning potential, owing to the passivation of the surface. In the third region, the current density began to increase again with the increasing scanning potential due to the destruction of the formed oxide films by overpotential.

Table 1 lists the E_{corr} and i_p. It is obvious that under both static corrosion and tribocorrosion conditions, the i_p of Ti-10Mo-xCu alloy was lower than that of CP Ti and Ti64 alloy. With increasing in Cu content, the i_p of Ti-10Mo-xCu alloys decreased initially and then increased. Among them, the Ti-10Mo-3Cu exhibited the lowest i_p of $0.195\pm0.02\times10^{-6}$ A/cm^2 and $0.93\pm0.05\times10^{-5}$ A/cm^2, respectively. In theory, with more Cu, the corrosion resistance of Ti-10Mo-xCu alloy enhances due to more β and Ti_2Cu intermetallic phases are generated [43, 44]. However, the corrosion resistance of Ti-10Mo-5Cu took on a downward trend instead. This is mainly because although Ti_2Cu can improve the corrosion resistance, it can also form galvanic cells with the α or β phase, which could reduce the corrosion resistance [45]. Compared with Ti-10Mo-3Cu alloy, there were more Ti_2Cu phases formed in Ti-10Mo-5Cu alloy, which can result in more galvanic cells formed in the Ti-10Mo-5Cu alloy. So, the corrosion resistance of Ti-10-3Cu was higher than the Ti-10Mo-5Cu alloy.

Additionally, it can be observed that the passive current density under the tribocorrosion conditions was generally higher than that under static corrosion conditions, indicating that mechanical wear can accelerate the corrosion process. As mentioned before, under the tribocorrosion conditions, the exfoliation of oxide films caused by sliding could expose the fresh-metal to the corrosive medium, thereby accelerating the corrosion process. In addition, galvanic corrosion occurring between the passivated areas (cathode) and the surrounding de-passivated areas (anode) under tribocorrosion conditions can also lead to an accelerated corrosion rate [46].

4. Conclusions

Ti-10Mo-xCu alloy was fabricated from a PM route in this study. The effects of Cu content on pure mechanical wear, electrochemical corrosion, and tribocorrosion of Ti-10Mo-xCu alloys were fully investigated. The main conclusions can be summarised as follows:

(1) The Vickers micro-hardness of Ti-10Mo-xCu increases with the Cu content, and the Ti-10Mo-5Cu alloy exhibits the highest hardness of 390.8±17.6 HV due to the solid strengthening by Mo and Cu elements.

(2) The passive current density of Ti-10Mo-xCu alloys decreases initially and subsequently increases with an increase in Cu content under both static corrosion and tribocorrosion conditions. The Ti-10Mo-3Cu alloy exhibits the lowest passive

current density of $0.195 \pm 0.02 \times 10^{-6}$ A/cm^2 and $0.93 \pm 0.05 \times 10^{-5}$ A/cm^2, respectively.

(3) The Ti-10Mo-5Cu alloy exhibits the lowest wear rate of 4.234±0.06 mm/y and 8.25033±0.11 mm/y under pure mechanical wear and tribocorrosion conditions respectively.

(4) A synergy interaction between wear and corrosion accelerated the materials loss greatly. The wear mechanisms for all the Ti-10Mo-xCu alloys are a combination of delamination, abrasion and adhesion wear.

Acknowledgments

This research work is supported by the National Natural Science Foundation of China (51922004, 51874037), State Key Lab of Advanced Metals and Materials, University of Science and Technology Beijing (2019-Z14). Fundamental Research Funds for the Central Universities (FRF-TP-19005C1Z). Chaozong Liu acknowledges the support from the European Commission via the H2020 MSCA RISE BAMOS programme (734156). Bo Su would like to thank the financial support from the MRC (MR/S010343/1) and the EU H2020 MSCA RISE Bio-TUNE programme. Wei Xu acknowledges the support from the China Scholarship Council (CSC) for a CSC Ph.D. scholarship (201906460106).

Data Availability

The data that support the findings of this study are available from the corresponding authors on reasonable request.

References

[1] D.L. Wise, D.J. Trantolo, D.E. Altobelli, M.J. Yaszemsk, J.D. Grasser, Human Biomaterials Applications, Humana Press, Totowa, NJ, 1996.

[2] M.J. Yaszemsk, D.J. Trantolo, K.U. Lewandrowski, V. Hasirci, D.E. Altobelli, D.L. Wise, Biomaterials in Orthopedics, Marcel Dekker Inc., New York, NY, 2004.

[3] W. Xu, X. Lu, J.J. Tian, C. Huang, M. Chen, Y. Yan, L.N. Wang, X.H. Qu, C.E Wen, Microstructure, wear resistance, and corrosion performance of Ti35Zr28Nb alloy fabricated by powder metallurgy for orthopedic applications, J. Mater. Sci. Technol. 41 (2020) 191-198.

[4] M. Geetha, A.K. Singh, R. Asokamani, A.K. Gogia, Ti-based biomaterials, the ultimate choice for orthopedic implants-A review, Prog. Mater. Sci. 54 (2009) 397-425.

[5] W. Xu, X. Lu, M.D. Hayat, J.J. Tian, C. Huang, M. Chen, X.H. Qu, C.E Wen, Fabrication and properties of newly developed Ti35Zr28Nb scaffolds fabricated by powder metallurgy for bone-tissue engineering, J. Mater. Res. Technol. 8 (2019), 3696-3704.

[6] W. Xu, X. Lu, L.N. Wang, Z.M. Shi, S.M. Lv, Q. Ma, X.H. Qu, Mechanical properties, in vitro corrosion resistance and biocompatibility of metal injection molded Ti-12Mo alloy for dental applications, J. Mech. Behav. Biomed. 88 (2018) 534-547

[7] B. Aksakal, O.S. Yildirim, H. Gul, Metallurgical failure analysis of various implant materials used in orthopedic applications, J. Fail. Anal. Prev. 4 (2004) 17-23.

[8] H. Kröger, P. Venesmaa, J. Jurvelin, H. Miettinen, O. Suomalainen, E. Alhava, Bone density at the proximal femur after total hip arthroplasty, Clin. Orthop. Relat. R. 352 (1998) 66-74.

[9] G. D. Bastiani, R. Aldegheri, L.R. Brivio, The treatment of fractures with a dynamic axial fixator, J. Bone Joint Surg. 66 (1984) 538-545.

[10] M. Deysine, Infections associated with surgical implants, N. Engl. J. Med. 351 (2004) 193-195

[11] W. Xu, C.J. Hou, Y.X. Mao, L. Yang, M. Tamaddon, J.L. Zhang, X.H. Qu, C.Z. Liu, B. Su, X. Lu, Characteristics of novel Ti-10Mo-xCu alloy by powder metallurgy for potential biomedical implant applications, Bioact. Mater. 5 (2020) 659-666.

[12] N.T.C. Oliveira, A.C. Guastaldi, Electrochemical stability and corrosion resistance of Ti-Mo alloys for biomedical applications, Acta Biomater. 5 (2009) 399-405.

[13] Y.Y. Chen, L.J. Xu, Z.G. Liu, F.T. Kong, Z.Y. Chen, Microstructures and properties of titanium alloys Ti-Mo for dental use, T Nonferr. Metal. Soc. 16 (2006), s824-s828.

[14] C.E.B. Marino, L.H. Mascaro, EIS characterization of a Ti-dental implant in artificial saliva media: dissolution process of the oxide barrier, J. Electroanal. Chem. 568 (2004) 115-120.

[15] Y. Yan, A. Neville, D. Dowson, Biotribocorrosion-an appraisal of the time dependence of wear and corrosion interactions: I. The role of corrosion, J. Phys. D. Appl. Phys. 39 (2006) 3200-3205.

[16] L. Kunčická, R. Kocich, T.C. Lowe, Advances in metals and alloys for joint replacement, Prog. Mater. Sci. 88 (2017) 232-280.

[17] M. Hussein, A. Mohammed, N. Al-Aqeeli, Wear characteristics of metallic biomaterials: a review, Materials 8 (2015) 2749-2768.

[18] W. Xu, J.J. Tian, Z. Liu, X. Lu, M.D. Hayat, Y. Yan, Z. Li, X.H. Qu, C.E Wen, Novel porous Ti35Zr28Nb scaffolds fabricated by powder metallurgy with excellent osteointegration ability for bone-tissue engineering applications, Mater. Sci. Eng. C-

Mater. 105 (2019) 110015.

[19] W. Xu, X. Lu, B. Zhang, C.C Liu, S.M. Lv, S.D. Yang, X.H. Qu, Effects of porosity on mechanical properties and corrosion resistances of PM-fabricated porous Ti-10Mo alloy, Metals, 8 (2018), 188-201.

[20] Y.K. Zhang, Q.Y. Yu, C. Yang, Corrosion and wear behaviors of medical Ti6Al4V alloy and the performance improvement, Electromachining Mould. 4 (2019) 49-53.

[21] Z. Doni, A.C Alves, F. Toptan, J.R Gomes, A. Ramalho, M. Buciumeanu, L. Palaghian, F.S. Silva, Dry sliding and tribocorrosion behaviour of hot pressed CoCrMo biomedical alloy as compared with the cast CoCrMo and Ti6Al4V alloys, Mater. Des. 52 (2013) 47-57.

[22] W. Xu, M. Li, C.E. Wen, S.M. Lv, C.C. Liu, X. Lu, X.H. Qu, The mechanical properties and in vitro biocompatibility of PM-fabricated Ti-28Nb-35.Zr alloy for orthopedic implant applications, Materials 11 (2018) 531-543.

[23] W. Xu, S.Q. Xiao, X. Lu, G. Chen, C.C. Liu, X.H. Qu, Fabrication of commercial pure Ti by selective laser melting using hydride-dehydride titanium powders treated by ball milling, J. Mater. Sci. Technol. 35 (2019) 322-327.

[24] ASTM G59-97, Standard test method for conducting potentiodynamic polarization resistance measurements, West Conshohocken, PA: ASTM International, 2014.

[25] ASTM E384-11, Standard Test Method for Knoop and Vickers Hardness of Materials, West Conshohocken, PA: ASTM International, 2011.

[26] J. Ureña, S. Tsipas, A.M. Pinto, F. Toptan, E. Gordo, A. Jiménez-Morales, Corrosion and tribocorrosion behaviour of β-type Ti-Nb and Ti-Mo surfaces designed by diffusion treatments for biomedical applications, Corros. Sci. 140 (2018) 51-60.

[27] ASTM G119-09, Standard Guide for Determining Synergism Between Wear and Corrosion, West Conshohocken, PA: ASTM International, 2016.

[28] K.N. Campo, E.S.N. Lopes, C.J. Parrish, R. Caram, Rapid quenching of semisolid Ti-Cu alloys: Insights into globular microstructure formation and coarsening, Acta Mater. 139 (2017) 86-95

[29] W. Xu, M. Chen, X. Lu, D.W. Zhang, H.P. Singh, J.S. Yu, Y. Pan, X.H. Qu, C.Z. Liu, Effect of Mo content on corrosion and tribocorrosion behaviours of Ti-Mo orthopaedic alloys fabricated by powder metallurgy, Corros. Sci. 2020, 108557.

[30] C. Ohkubo, I. Shimura, T. Aoki, S. Hanatani, T. Hosoi, M. Hattori, Y. Oda, T. Okabe, Wear resistance of experimental Ti-Cu alloys, Biomaterials, 24 (2003) 3377-3381.

[31] E.L. Zhang, J. Ren, S.Y. Li, L. Yang G.W. Qin, Optimization of mechanical properties, biocorrosion properties and antibacterial properties of as-cast Ti-Cu alloys, Biomed, Mater. 11(2016) 065001.

[32] R. Dong, W.W. Zhu, C.C. Zhao, Y.W. Zhang, F.Z. Ren, Microstructure, mechanical properties, and sliding wear behavior of spark plasma sintered Ti-Cu alloys, Metall Mater. Trans. A 49 (2018), 6147-6160.

[33] B.B. Zhang, J.Z. Wang, F.Y. Yan, Load-dependent tribocorrosion behaviour of nickel-aluminium bronze in artificial seawater, Corros. Sci. 131 (2018) 252-263.

[34] Y. Z. Ding, D.C. Zhu, X.N. Ge, Effect of Cu on microstructure and hardness of Ti-10Mo dental alloy, Hot Working Technol. 41 (2012) 33-36.

[35] A.F. Yetim, Investigation of wear behavior of titanium oxide films, produced by anodic oxidation, on commercially pure titanium in vacuum conditions, Surf. Coat. Tech. 205 (2010) 1757-1763.

[36] C. Yan, Q.F. Zeng, Y.T. Xu, W.J. He, Microstructure, phase and tribocorrosion behavior of 60NiTi alloy, Appl. Surf. Sci. 498 (2019) 143838.

[37] J. Ureña, E. Tabares, S. Tsipas, A. Jiménez-Morales, E. Gordo, Dry sliding wear behaviour of β-type Ti-Nb and Ti-Mo surfaces designed by diffusion treatments for

biomedical applications, J. Mech. Behav. Biomed. 91 (2019) 335-344.

[38] V.G. Pina, V. Amigó, A.I. Muñoz, Microstructural, electrochemical and tribo-electrochemical characterisation of titanium-copper biomedical alloys, Corros. Sci. 109 (2016) 115-125.

[39] W. Xu, A.H. Yu, X. Lu, M. Tamaddon, L.Q. Ng, M.D. Hayat, M.D. Wang, J.L. Zhang, X.H. Qu, C.Z. Liu, Synergistic interactions between wear and corrosion of Ti-16Mo orthopedic alloy, J. Mater. Res. Technol. 9 (2020): 9996-10003

[40] J. Chen, F.Y. Yan, B.B. Chen, J.Z. Wang, Assessing the tribocorrosion performance of Ti-6Al-4V, 316 stainless steel and Monel K500 alloys in artificial seawater, Mater. Corros. 64 (2013) 394-401.

[41] W. Xu, Z. Liu, X. Lu, J.J.Tian, G. Chen, B.W. Liu, Z. Li, X.H. Qu, C.E Wen, Porous Ti-10Mo alloy fabricated by powder metallurgy for promoting bone regeneration, Sci. China Mater. 62 (2019), 1053-1064.

[42] Z. Doni, A.C. Alves, F. Toptan, L.A. Rocha, M. Buciumeanu, Tribocorrosion behavior of hot pressed CoCrMo-HAP biocomposites, Tribol. Int. 91 (2015) 221-227.

[43] S. Karimi, T. Nickchi, A. Alfantazi, Effects of bovine serum albumin on the corrosion behaviour of AISI 316L, Co-28Cr-6Mo, and Ti-6Al-4V alloys in phosphate buffered saline solutions, Corros. Sci. 53 (2011) 3262-3272.

[44] M. Niinomi, Recent metallic materials for biomedical applications, Metall. Mater. Trans. A 33 (2002) 477-486.

[45] S. Guo, Y.J. Lua, S.Q. Wu, L.L. Liu, M.J. He, C.Q. Zhao a, Y.L. Gan, J.J. Lina, J.S. Luo, X.C. Xu, J.X. Lin, Preliminary study on the corrosion resistance, antibacterial activity and cytotoxicity of selective-laser-melted Ti6Al4V-xCu alloys, Mater. Sci. Eng. C-Mater. 72 (2017) 631-640.

[46] Y. Bai, X. Gai, S. Li, L.C. Zhang, Y. Liu, Y.L. Hao, X. Zhang, R. Yang, Y Gao, Improved corrosion behaviour of electron beam melted Ti-6Al-4V alloy in phosphate buffered saline, Corros. Sci. 123 (2017) 289-296.

Figure and table captions

Fig. 1 XRD patterns (a) and Vickers micro-hardness (b) of Ti-10Mo-xCu alloys with different Cu content, alongside with the CP Ti, and Ti64 alloy for comparison

Fig. 2 The COF of Ti-10Mo-xCu, alongside with CP Ti and Ti64 alloy in PBS solution at 37 ± 0.5 ℃ under (a) pure mechanical wear and (b) tribocorrosion

Fig. 3 3D surface morphologies recorded on Ti-10Mo-xCu, CP Ti, and Ti64 alloy after pure mechanical wear (a-f) and tribocorrosion (g-l) tests: (a) and (g) Ti-10Mo; (b) and (h) Ti-10Mo-1Cu; (c) and (i) Ti-10Mo-3Cu; (d) and (j) Ti-10Mo-5Cu; (e) and (k) CP Ti; (f) and (l) Ti64

Fig. 5 SEM and EDS analysis of Ti-10Mo-xCu alloys, alongside with the CP Ti, and Ti64 after pure mechanical wear (a-f) and tribocorrosion (g-i) tests: (a) and (g) Ti-10Mo; (b) and (h) Ti-10Mo-1Cu; (c) and (i) Ti-10Mo-3Cu; (d) and (j) Ti-10Mo-5Cu; (e) and (k) CP Ti; (f) and (l) Ti64

Fig. 6 OCP vs. time curves for Ti-10Mo-xCu, alongside with the CP Ti and Ti64 alloy before static corrosion test in PBS solution at 37 ± 0.5 ℃

Fig. 7 OCP vs. time curves for the Ti-10Mo-xCu, alongside with the CP-Ti and Ti64 alloy before, during, and after sliding in PBS solution at 37 ± 0.5 ℃

Fig. 8 Repassivation rate of Ti-10Mo alloys with different Cu contents, CP-Ti alloy, and Ti64 alloy

Fig. 9 The potentiodynamic polarisation curves of Ti-10Mo-xCu, alongside with the CP Ti, and Ti64 alloy under (a) static corrosion and (b) tribocorrosion conditions

Table 1 Obtained corrosion parameters from the PD curves of Ti-10Mo-xCu, alongside with the CP Ti, and Ti64 alloy under static corrosion and tribocorrosion conditions

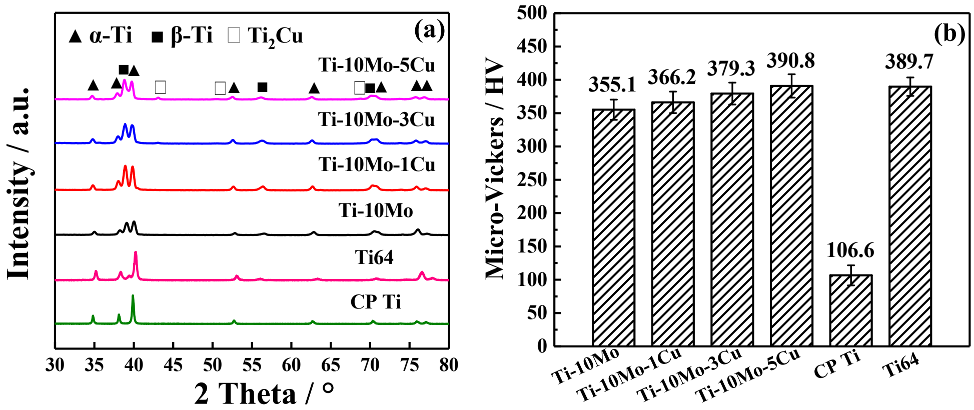

Fig. 1 XRD patterns (a) and Vickers micro-hardness (b) of Ti-10Mo-xCu alloys with different Cu content, alongside with the CP Ti, and Ti64 alloy for comparison

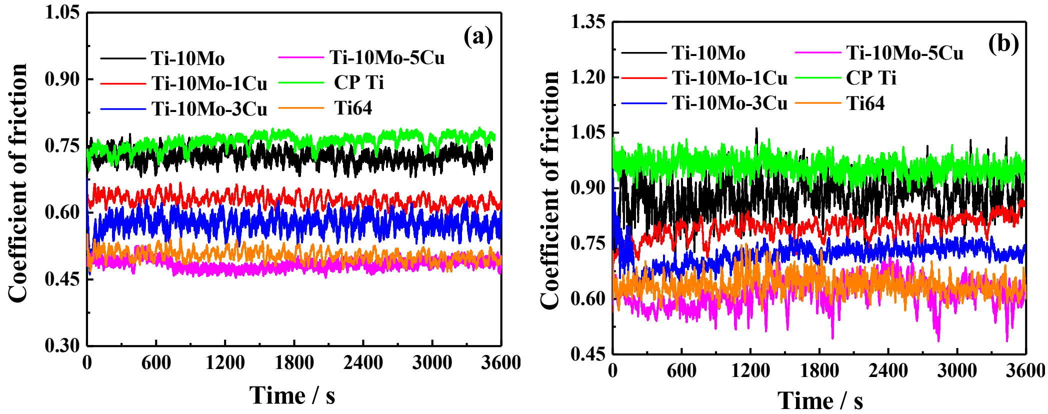

Fig. 2 The COF of Ti-10Mo-xCu, alongside with CP Ti and Ti64 alloy in PBS solution at 37 ± 0.5 °C under (a) pure mechanical wear and (b) tribocorrosion

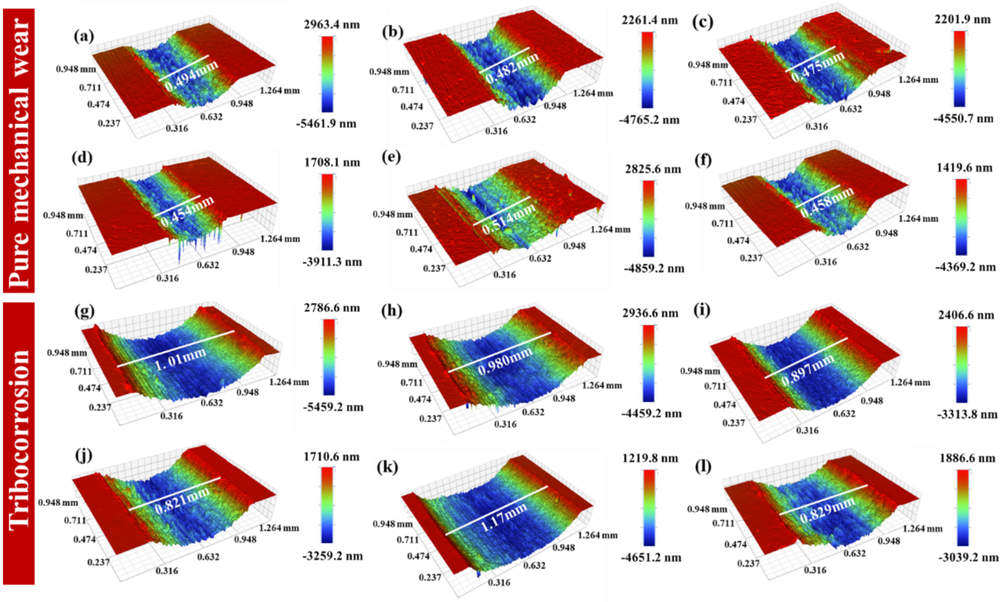

Fig. 3 3D surface morphologies recorded on Ti-10Mo-xCu, CP Ti, and Ti64 alloy after pure mechanical wear (a-f) and tribocorrosion (g-l) tests: (a) and (g) Ti-10Mo; (b) and (h) Ti-10Mo-1Cu; (c) and (i) Ti-10Mo-3Cu; (d) and (j) Ti-10Mo-5Cu; (e) and (k) CP Ti; (f) and (l) Ti64

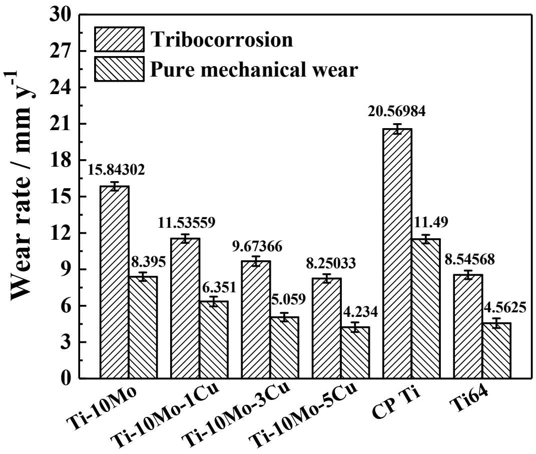

Fig. 4 Wear rate of Ti-10Mo-xCu, CP-Ti, and Ti64 under pure mechanical wear and tribocorrosion test conditions

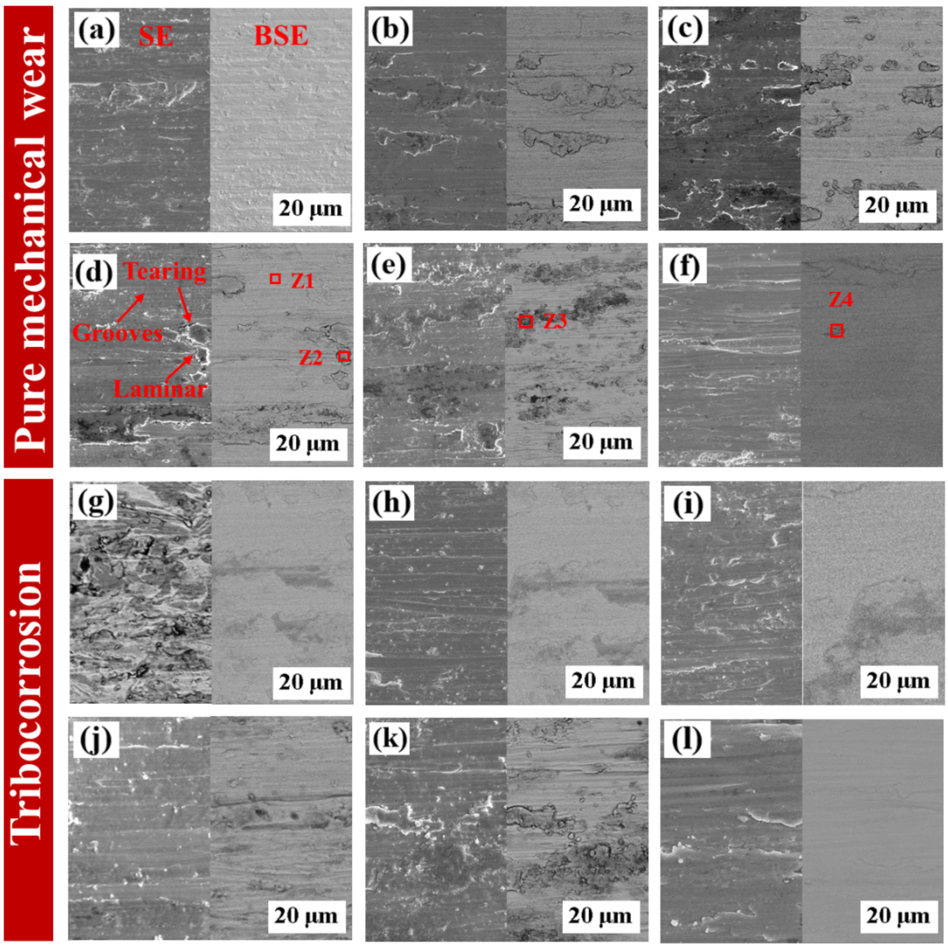

(m)

Marked areas	Ti (wt%)	Mo (wt%)	O (wt%)	Al (wt%)	V (wt%)	Cu(wt%)
Z1	84.75	10.32	0	---	---	4.93
Z2	69.97	10.22	14.66	---	---	5.15
Z3	73.37	---	26.73	---	---	---
Z4	74.31	---	13.38	6.77	5.54	---

Fig. 5 SEM and EDS analysis of Ti-10Mo-xCu alloys, alongside with the CP Ti, and Ti64 after pure mechanical wear (a-f) and tribocorrosion (g-i) tests: (a) and (g) Ti-10Mo; (b) and (h) Ti-10Mo-1Cu; (c) and (i) Ti-10Mo-3Cu; (d) and (j) Ti-10Mo-5Cu; (e) and (k) CP Ti; (f) and (l) Ti64; (m) EDS results of Z1, Z2, Z3, and Z4

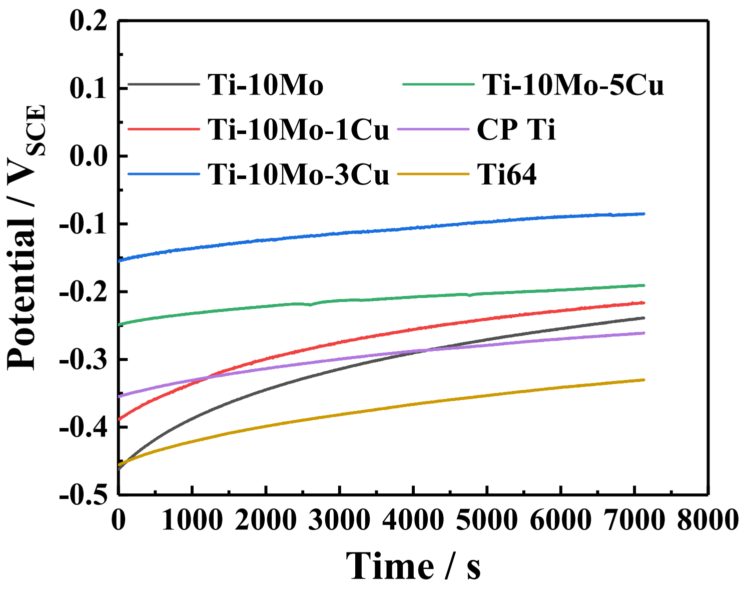

Fig. 6 OCP vs. time curves for Ti-10Mo-xCu, alongside with the CP Ti and Ti64 alloy before static corrosion test in PBS solution at 37 ± 0.5 ℃

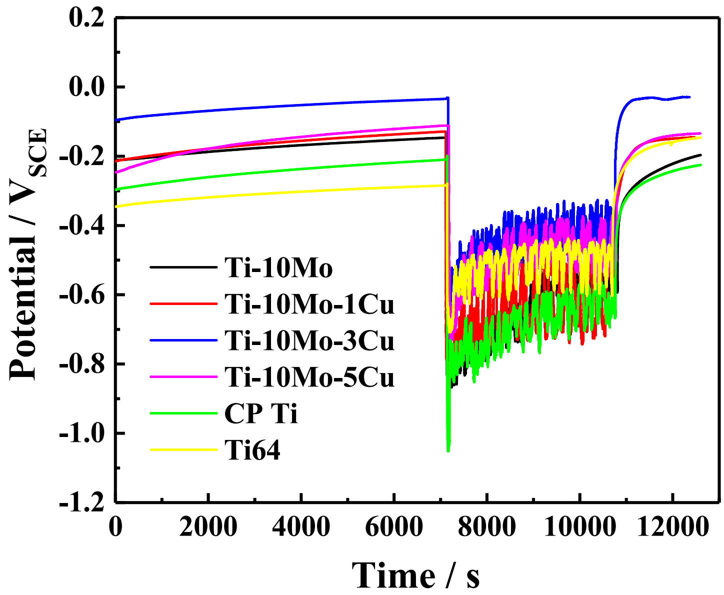

Fig. 7 OCP vs. time curves for the Ti-10Mo-xCu, alongside with the CP-Ti and Ti64 alloy before, during, and after sliding in PBS solution at 37 ± 0.5 ℃

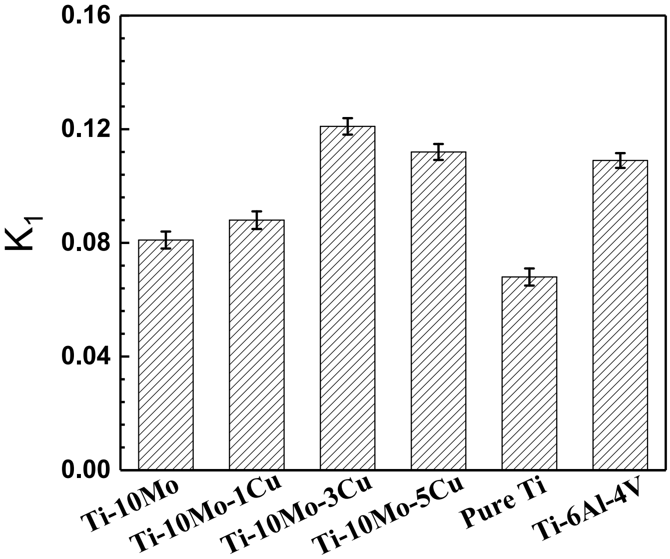

Fig. 8 Repassivation rate of Ti-10Mo alloys with different Cu contents, CP-Ti alloy and Ti64 alloy

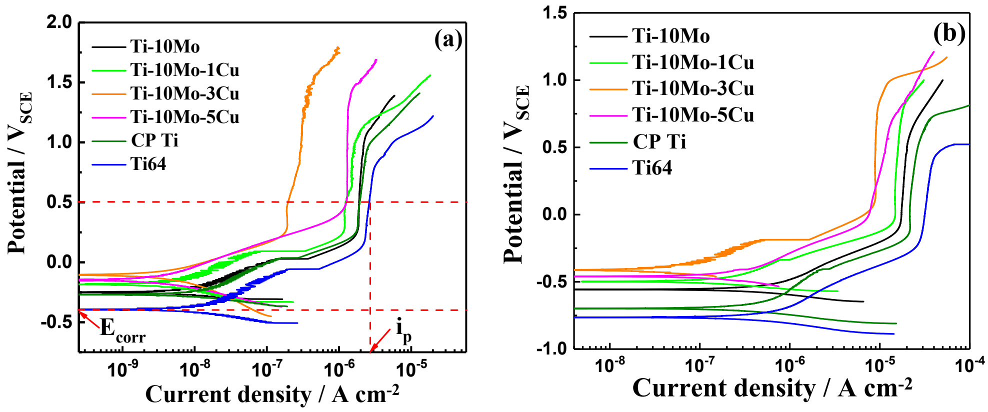

Fig. 9 The potentiodynamic polarisation curves of Ti-10Mo-xCu, alongside with the CP Ti, and Ti64 alloy under (a) static corrosion and (b) tribocorrosion conditions

Table 1 Obtained corrosion parameters from the PD curves of Ti-10Mo-xCu, alongside with the CP Ti, and Ti64 alloy under static corrosion and tribocorrosion conditions

	Static corrosion		Tribocorrosion	
Alloy	E_{corr} (V)	$i_p \times 10^{-6}$ (A/cm^2)	E_{corr} (V)	$i_p \times 10^{-5}$ (A/cm^2)
Ti-10Mo	-0.249±0.05	1.89±0.05	-0.556±0.09	2.02±0.06
Ti-10Mo-1Cu	-0.185±0.02	1.27±0.06	-0.491±0.11	1.61±0.04
Ti-10Mo-3Cu	-0.106±0.01	0.195±0.02	-0.408±0.12	0.93±0.05
Ti-10Mo-5Cu	-0.154±0.02	1.25± 0.04	-0.455±0.08	1.15±0.08
CP Ti	-0.279±0.06	1.94± 0.06	-0.701±0.19	2.75±0.12
Ti64	-0.395±0.08	2.67± 0.07	-0.766±0.22	5.29±0.15

Conflict of interest

The authors declare that they have no known competing for financial interests or personal relationships that could have appeared to influence the work reported in this paper.

Author Statement

Xin Lu: Conceptualization, Data curation, Formal analysis, Writing - original draft, Writing - review & editing, Supervision, Project administration; Dawei Zhang: Investigation, Writing - review & editing; Wei Xu: Conceptualization, Data curation, Formal analysis, Writing - original draft, Writing - review & editing; Aihua Yu: Data curation, Formal analysis, Investigation; Jiazhen Zhang: Investigation, Writing - review & editing; Maryam Tamaddon: Investigation, Writing - review & editing; Jianliang Zhang: Investigation, Writing - review & editing; XuanHui Qu: Formal analysis, Investigation; Chaozong Liu: Formal analysis, Investigation; Bo Su: Investigation, Writing - review & editing.